

## Crystal Engineering | Hot Paper |

Proton in a Confined Space: Synthesis of  $\text{H}^+ \subset \text{Crypt-111}$  Iodide and some Halogen-Bonded DerivativesVijith Kumar,<sup>[a]</sup> Tullio Pilati,<sup>[a]</sup> Silvio Quicik,<sup>[b]</sup> Michele R. Chierotti,<sup>[c]</sup> Carlo Nervi,<sup>[c]</sup> Roberto Gobetto,<sup>[c]</sup> and Giuseppe Resnati<sup>\*[a]</sup>

**Abstract:** Experimental observations and modeling data are reported on the solid-state structural features of crypt-111-HI (**1**) and the three-component co-crystals that **1** forms with  $\alpha,\omega$ -diiodoperfluoroalkanes **2a–d**. X-ray analyses indicate that, in all five systems and at low temperature, the caged proton is covalently bonded to a single nitrogen atom and is involved in a network of intramolecular hydrogen bonds. In contrast, room-temperature, solid-state  $^{15}\text{N}$  NMR spectroscopy suggests magnetic equivalency of the two N atoms of crypt-111 in both **1** and co-crystals of **1** with diiodoperfluoroalkanes. Computational modelling confirms that the acidic hydrogen inside the cavity preferentially sits

along the internitrogen axis and is covalently bonded to one nitrogen. The computed energy barriers suggest that the hopping of the encapsulated proton between the two N atoms of the cage can occur in the halogen-bonded co-crystals of **1·2**, but it is less evident in the pure  $\text{H}^+ \subset \text{crypt-111}$  iodide **1**. These different pictures of the proton position and dynamics obtained by using different techniques and conditions confirm the unique characteristics of the confined space within the cavity of crypt-111 and the distinctive features of processes occurring therein.

Most of the present knowledge on chemical phenomena is related to molecules dwelling in open three dimensional (3D) space for example, of a gas or a liquid phase. This information typically loses most of its validity when molecules are in a confined space. For instance, when reactions take place within a two dimensional (2D) space, for example, when the reagents are adsorbed on a solid–liquid or solid–vacuum interface, the composition and morphology of the surface may allow for sluggish or prohibited reactions to proceed efficiently and unique selectivities may be observed.<sup>[1]</sup> Also one dimensional (1D) confined spaces offer distinctive opportunities, for example, the synthesis of nanorods in the nanochannels of or-

ganic or inorganic membranes.<sup>[2]</sup> When molecules are restrained in a cage, a zero-dimensional (0D) confined space, their motion is mostly restricted and intermolecular interactions can be amplified<sup>[3]</sup> or the half-life of fleeting and reactive species can be extended.<sup>[4]</sup> In a cage, binding characteristics<sup>[5]</sup> as well as reactivity<sup>[6]</sup> and catalysis<sup>[7]</sup> may gain strong improvements in rate, selectivity, and yields. Unique and useful results can thus be achieved in different fields such as materials fabrication by self-assembly,<sup>[8]</sup> structural characterization at the nanogram scale,<sup>[9]</sup> and assessment of the mechanism-of-action of new drugs.<sup>[10]</sup>

Proton transfer is probably one of the most ubiquitous processes in chemical systems. It continuously occurs in water,<sup>[11]</sup> is a crucial step in many reactions,<sup>[12]</sup> plays a key role in the action mechanism of small molecules and complex macromolecules of biological interest,<sup>[13]</sup> and impacts the structure and properties of molecular and polymeric materials.<sup>[14]</sup> Single, dual, and multiple proton transfer, either stepwise or correlated have been observed; the occurrence of a given phenomenon being dependent on the involved (macro)molecule(s) and the environment. The distinctive features of proton transfer in a confined space have also been studied both in artificial and natural systems<sup>[15]</sup> and phenomena as distinctive as proton tunneling have been noted.<sup>[11b,16]</sup>

4,10,15-Trioxa-1,7-diazabicyclo[5.5.5]heptadecane (crypt-111), the smallest cryptand and an effective proton sponge, was first reported in 1972 by Cheney and Lehn.<sup>[17a]</sup> The most stable conformation of crypt-111, which directs the two nitrogen lone pairs inside the cavity (*in-in* conformation),<sup>[18]</sup> is a rather weak base ( $\text{p}K_{\text{a}1}=7.1$ ). Under kinetic control monoprotonation

[a] Dr. V. Kumar, Dr. T. Pilati, Dr. G. Resnati  
Nanostructured Fluorinated Materials Laboratory (NFMLab)  
Department of Chemistry, Materials and Chemical Engineering "Giulio Natta"  
Politecnico di Milano  
Via L. Mancinelli 7  
20131 Milan (Italy)  
E-mail: giuseppe.resnati@polimi.it

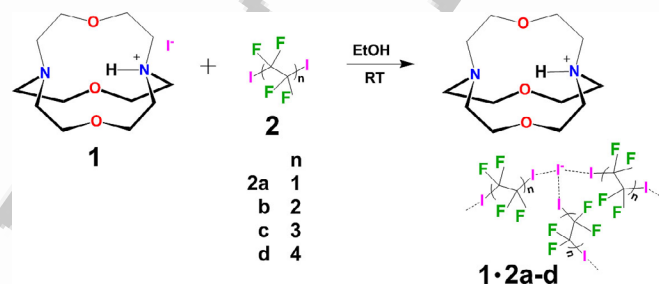
[b] Dr. S. Quicik  
CNR, Istituto di Scienze e Tecnologie Molecolari  
via C. Golgi 19  
20133 Milan (Italy)

[c] Dr. M. R. Chierotti, Dr. C. Nervi, Dr. R. Gobetto  
Department of Chemistry and NIS  
University of Turin  
via P. Giuria 7  
10125 Turin (Italy)

Supporting information and the ORCID identification number(s) for the author(s) of this article can be found under:  
<https://doi.org/10.1002/chem.201701699>.

occurs outside the cavity with a fast inversion of configuration at one nitrogen, and the formed *in-out*<sup>+</sup> cation can be further protonated, with a second inversion at nitrogen, to give the *out*<sup>+</sup>–*out*<sup>+</sup> dication ( $pK_{a2} \approx 1$ ) or can slowly convert ( $k = 2.3 \times 10^{-4} \text{ s}^{-1}$ ) into the more stable conformer bearing the proton inside the cavity (*in-in*<sup>+</sup> or  $\text{H}^+\text{crypt-111}$  monocation). As a further indication of the unique kinetic and thermodynamic properties of a proton inside the cavity of crypt-111, the reaction  $\text{H}_2\text{O} + \text{crypt-111}(\text{in-in}) \rightleftharpoons \text{OH}^- + \text{H}^+\text{crypt-111}$  has a  $\Delta G^\circ \leq 20 \text{ kJ mol}^{-1}$ ; thus water dissociation is highly favored in the presence of crypt-111 that is favored by proton encapsulation. Crypt-111 can also bear two protons inside the cavity (*in*<sup>+</sup>–*in*<sup>+</sup> or  $2\text{H}^+\text{crypt-111}$  dication) and the thermodynamic stability of the second protonation is similar to that of ordinary tertiary amines (the reaction  $\text{H}_2\text{O} + \text{H}^+\text{crypt-111} \rightleftharpoons \text{OH}^- + 2\text{H}^+\text{crypt-111}$  has a  $\Delta G^\circ \approx 35 \text{ kJ mol}^{-1}$ ). The combination of these and other properties enables for the use of  $\text{H}^+\text{crypt-111}$  as a “molecular burette”, in other words a molecular device for the slow and continuous release of protons and automatic titrations monitored using spectrophotometric<sup>[19]</sup> or nuclear magnetic resonance (NMR) techniques.<sup>[20]</sup>

The readily available information on crypt-111 protonation in solution contrasts with the poor information available on the structural and dynamic aspects of protonated crypt-111 in the solid state. No atomic coordinates are available in the Cambridge Structural Database (CSD, ConQuest 1.19 version) for  $\text{H}^+\text{crypt-111}$  species,<sup>[21]</sup> with only selected data for  $\text{H}^+\text{crypt-111}$  picrate being reported.<sup>[22]</sup> The proton location and motion in other proton sponges, for example, 1,8-dimethylaminonaphthalene<sup>[23]</sup> and its analogues,<sup>[24]</sup> have been extensively studied, but the same features have never been investigated for  $\text{H}^+\text{crypt-111}$  in the solid state. Herein we describe some experimental observations and theoretical calculations on the  $\text{H}^+\text{crypt-111}$  cation. Specifically, we report the single crystal X-ray structure, the <sup>15</sup>N CPMAS spectra, and some modelling of  $\text{H}^+\text{crypt-111}$  iodide **1** and its adducts **1·2a–d** where the iodide anion is halogen bonded to  $\alpha,\omega$ -diiodoperfluoroalkanes **2a–d** (Scheme 1). Different results regarding the proton position and dynamics are obtained depending on the technique used, possibly as a consequence of the different time scales and temperatures employed. Moreover, the  $\text{H}^+\text{crypt-111}$  cation seems to have an energetically quite flat conformational landscape, and this feature is also influential on the structural characteristics of the studied systems confirming the tendency



**Scheme 1.** Chemical formulas of starting tectons **1** and **2a–d**, and formed three-component co-crystals **1·2a–d**.

of crypt-111 to induce unique characteristics in processes occurring within its cavity.<sup>[25]</sup>

## Results and Discussion

### Structural characterization of $\text{H}^+\text{crypt-111}$ iodide (**1**)

$\text{H}^+\text{Crypt-111}$  iodide was prepared following reported procedures<sup>[26]</sup> and crystals suitable for single crystal analyses were obtained through isothermal evaporation of an ethanol solution. Diffraction data for  $\text{H}^+\text{crypt-111}$  iodide **1** and its halogen-bonded co-crystals **1·2a–d** were all collected at 100 K and were good enough to allow for an assessment of the structural details of the of  $\text{H}^+\text{crypt-111}$  moiety. Importantly, the acidic proton inside the cryptand cavity was experimentally located from the Fourier difference map.

$\text{H}^+\text{Crypt-111}$  iodide **1** is in the hexagonal  $P6_3/m$  space group with  $Z=2$ . The crystal shows high symmetry that is related to the mirror plane through the three oxygen atoms of crypt-111. The cation adopts an *in-in*<sup>+</sup> conformation (Figure 1)

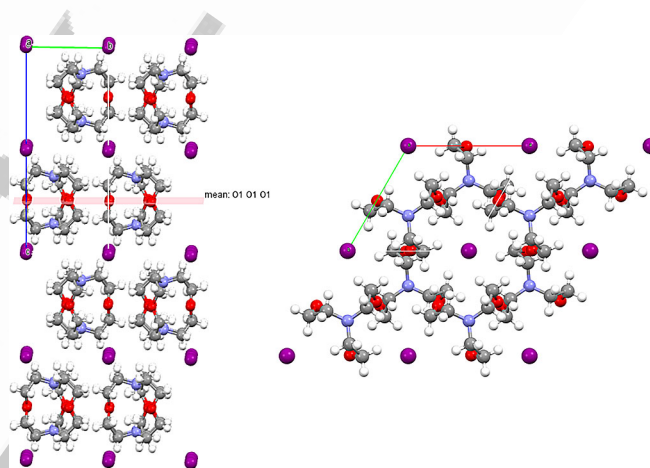


**Figure 1.** Partial ball-and-stick representation (Mercury 3.9) of the crystal packing of  $\text{H}^+\text{crypt-111}$  iodide **1** along *c* (right) and approximately along *a* (left). The mirror plane through the oxygen atoms is represented in pink. The hydrogen atoms on nitrogen atoms correspond to a 50% occupancy. Color codes: gray, carbon; white, hydrogen; blue, nitrogen; red, oxygen; magenta, iodine.

with a rugby-ball shape (intramolecular N–N and O–O separations are 369.6 and 364.7 pm, Table S.4 in the Supporting Information). *In-out*<sup>+</sup> and *out-out*<sup>+</sup> conformations have been observed in solution,<sup>[17]</sup> but the *in-in* arrangement is the most stable for the free cryptand and the protonated derivatives in the gas,<sup>[18]</sup> liquid,<sup>[17]</sup> and solid<sup>[22]</sup> phases. The nitrogen atoms adopt a distorted tetrahedral conformation ( $\angle \text{C–N–C} = 112.90^\circ$ ).

The encapsulated proton is observed the Fourier difference map on the axis bisecting the two nitrogen atoms. The  $\text{H}^+\text{crypt-111}$  is centered on the 3/m special position and the proton is consequently split over two equipopulated positions around the mirror plane. This disordered proton was refined with a fixed distance of 93 pm from the N atom. This splitting may result from an orientational disorder

of the  $\text{H}^+\text{crypt-111}$  moiety in the crystal packing where it is adopting two alternating dispositions relative to the mirror plane that bisects the three oxygen atoms. Alternatively the disorder may result from hopping of the hydrogen between the nitrogen atoms of a cryptand molecule. This latter possibility was unlikely as the barrier height for the process has been computed as high as  $17 \text{ kcal mol}^{-1}$ .<sup>[27]</sup> To rule out this possibility, we decided to pursue further information and to analyze the three-component co-crystals **1-2a-d** on the assumption that the expected lower symmetry of these systems might prevent orientational disorder.

### Structural characterization of co-crystals **1-2a-d**

#### Preparation

When 4,7,13,16,21,24-hexaoxa-1,10-diazabicyclo[8.8.8] hexacosane (crypt-222) encapsulates the cation of alkaline halides, halogen bonded<sup>[28]</sup> adducts are frequently obtained upon self-assembly with iodoperfluorocarbons<sup>[29]</sup> and other halogen bond (XB) donors.<sup>[30]</sup> Probably, cation cryptation boosts the electron-donor ability of halides and enables them to work as effective XB acceptors (donors of electron density). We expected that iodide anions of **1** would behave as naked anions and showcase an XB-acceptor ability as good as that of cation<sup>+</sup> crypt-222 iodides. Indeed, upon slow isothermal evaporation at room temperature of ethanol solutions containing cryptand **1** and bis-homologue  $\alpha,\omega$ -diiodoperfluorocarbons **2a-d** in a 1:1.5 ratio, the three-component co-crystals **1-2a-d** were obtained. This starting tecton ratio was used because co-crystals with this stoichiometry are typically obtained upon self-assembly of cation<sup>+</sup> crypt-222 iodides with  $\alpha,\omega$ -iodoperfluorocarbons.<sup>[28,29]</sup>

Melting points of **1-2a-d** were sharp and different from starting tectons **1** and **2a-d**, thus confirming the expected formation of supramolecular adducts rather than physical mixtures. IR spectra of **1-2a-d** showed the presence of peaks of both **1** and **2a-d** and the changes in peak frequency and intensity were consistent with the presence of XB.<sup>[28,29]</sup> For instance, the  $\nu_{\text{C-F}}$  stretching peaks at  $1147$  and  $1096 \text{ cm}^{-1}$  in **2a** and at  $1192$  and  $1128 \text{ cm}^{-1}$  in **2b** were located at  $1112$  and  $1082 \text{ cm}^{-1}$  in **1-2a** and at  $1178$  and  $1116 \text{ cm}^{-1}$  in **1-2b**. Similar redshifts for peaks in the  $1200\text{--}1000 \text{ cm}^{-1}$  region were shown for **1-2c,d** compared to non-complexed **2c,d** (Table S.1 in the Supporting Information).

#### Structural characterization of the supramolecular anions

Single-crystal X-ray analyses show that some of the structural features of the supramolecular anions are the same in all the three-component co-crystals **1-2a-d**, whereas some others are common to **1-2b-d** only; the three systems are mutually similar. For instance, **1-2a-d** crystallize in the triclinic  $P<\bar{C}>1$  space group and  $Z$  is 2 in **1-2a** and 1 in **1-2b-d**. Confusion of  $Z$  vs.  $Z'$ ?  $Z=2$  for  $P-1$  but  $Z=1$  for  $P1$ ? Two of the unit cell axes are nearly the same in **1-2b-d**, (the  $a$  and  $b$  dimensions differ by between  $10.81\text{--}10.95$  and  $11.03\text{--}11.05 \text{ pm}$ , respectively) indicating similarities in those two ori-

entations. In contrast, the  $c$  axis increases with the perfluoroalkyl chain length and varies from  $13.50 \text{ pm}$  in **1-2b** to  $16.84 \text{ pm}$  in **1-2d**.

Along with the cation-anion electrostatic attractions, the  $\text{C}\cdots\text{I}\cdots\text{I}^-$  XBs are by far the strongest interactions in the systems and are responsible for the self-assembly of iodide **1** with diiodoperfluorocarbons **2a-d**.<sup>[28,29]</sup> As expected, iodide anions in **1-2a-d** behave as tridentate donors of electron density and bind three different iodine atoms belonging to three distinct perfluoroalkyl chains, which, in turn work as bidentate and telchellic acceptors of electron density. Similarly to analogous systems and as expected for strong XBs,<sup>[28,29]</sup>  $\text{I}\cdots\text{I}^-$  interactions are quite short and approximately aligned with the  $\text{C}\cdots\text{I}$  covalent bond in all four co-crystals. Specifically,  $\text{I}\cdots\text{I}^-$  separations and  $\angle\text{C}\cdots\text{I}\cdots\text{I}^-$  angles span the ranges  $345.4\text{--}351.9 \text{ pm}$  and  $167.80^\circ\text{--}178.68^\circ$ , respectively. These separations are longer than the average covalent  $\text{I}\cdots\text{I}$  bond ( $266.6 \text{ pm}$ ) but shorter than the sum of van der Waals radius for an iodine atom ( $198 \text{ pm}$ ) and the Pauling ionic radius for an iodide anion ( $216 \text{ pm}$ ). (These separations correspond to normalized contacts  $Nc^{[31]}$  varying from  $0.83\text{--}0.85$ .) The three XBs around iodide ions define a distorted triangle and fairly planar pattern as the three  $\angle\text{I}\cdots\text{I}^-$  angles vary in the ranges  $70.71^\circ\text{--}77.32^\circ$ ,  $130.30^\circ\text{--}137.73^\circ$ , and  $144.16^\circ\text{--}156.46^\circ$ .

In the crystal packing of **1-2a**, diiodoperfluoroethane molecules and iodide anions give rise to halogen-bonded hexagonal systems forming helices which develop along the crystallographic  $b$  axis and have six iodide anions and six diiodoethane molecules along the pitch of the helix (Figure 2, top). In contrast, the crystal packing of **1-2b** co-crystals contains parallel ribbons of halogen-bonded anions and supramolecular anions formed by rhombic frames wherein iodide anions and iodoperfluorocarbons are the vertexes and the sides, respectively (Figure 2, bottom). Co-crystals **1-2c,d** present supramolecular anionic ribbons similar to **1-2b**.

The formation of remarkably short and directional XBs in **1-2a-d** co-crystals is a clear indication that crypt-111 is quite effective in cryptating the proton of hydrogen iodide and in

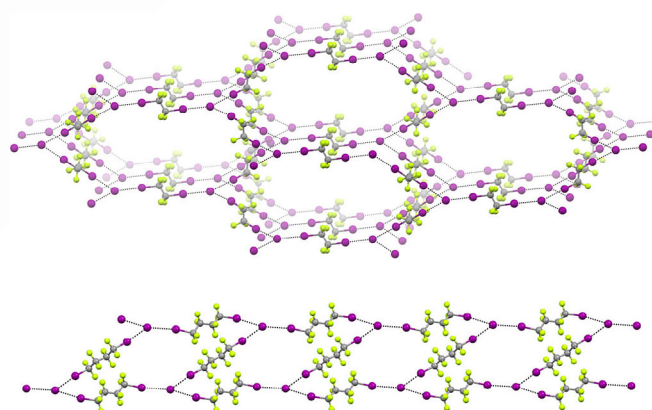


**Figure 2.** Ball-and-stick representation (Mercury 3.9) of the supramolecular anion in **1-2a** (top) and **1-2b** (bottom). The views approximately along the  $b$  axis (top) and along the  $a$  axis (bottom) show the hexagonal-helical system and the ribbon, respectively. Color codes: Gray, carbon; green, fluorine; magenta, iodine; black dotted lines, halogen bonds.



generating naked and nucleophilic iodide anions. This behavior parallels the ability of crypt-222 to form naked and nucleophilic iodides from alkaline iodides and may lead to numerous and useful synthetic opportunities.

Perfluoroalkyl derivatives have a strong tendency to segregate from both polar and apolar compounds and this tendency increases with the length of the perfluorinated chain.<sup>[32]</sup> It is thus not surprising that in the overall crystal packing of **1-2b-d**, the fluorinated ribbons further organize into fluorinated and anionic layers which alternate with hydrocarbon and cationic layers (Figure 3).

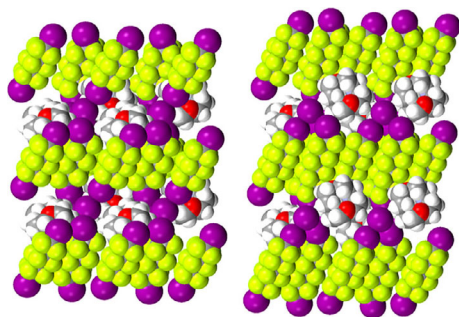


**Figure 3.** Space-filling representation (Mercury 3.9) of the overall crystal packing of co-crystals **1-2c** (left) and **1-2d** (right) along the crystallographic *a* axis showing the segregation of supramolecular anions. Color code: Gray, carbon; white, hydrogen; green, fluorine; red, oxygen; magenta, iodine.

### Structural characterization of supramolecular cation $H^+ \text{crypt-111}$

Some structural features of cation  $H^+ \text{crypt-111}$  in co-crystals **1-2a-d** and in pure  $H^+ \text{crypt-111}$  iodide **1** are similar, and others are not. Co-crystals **1-2a-d** have a lower symmetry than pure **1** and this may be the cause for the lower symmetry adopted by the  $H^+ \text{crypt-111}$  cation in **1-2a-d** than in **1**. Moreover, as it is the case for the respective halogen-bonded supramolecular anions, the  $H^+ \text{crypt-111}$  cation has very similar structures in co-crystals **1-2b-d** whereas it shows some unique characteristics in **1-2a**. In all four co-crystals **1-2a-d** the cryptand adopts the thermodynamically more stable *in-in* conformation with the two N atom lone pairs directed inward toward the cavity and adopting a distorted tetrahedral conformation ( $\angle \text{C-N-C}$  angles span the range  $111.01^\circ$ – $116.64^\circ$ , Table S.4). Two different such supramolecular cations are present in the unit cell of **1-2a** and both of them assume a more elongated shape than in **1**. In contrast, the cation adopts a single conformation in the unit cell of **1-2b-d** and it has a significantly less elongated conformation than in **1-2a** and pure **1** (the mean values of intramolecular N–N and O–O separations are 380.5 and 349.2 pm in **1-2a** and 303.5 and 416.0 pm in **1-2b-d**, respectively). The Fourier difference map gives a definitive location for the acidic hydrogen inside the cavity, which is bonded to one nitrogen atom (the N–H separations from the Fourier difference map are 85 pm for both the independent units in **1-2a** and 93, 99, and 88 pm for **1-2b**, **1-2c**, and **1-2d**, respectively). Three intramolecular H–O hydrogen bonds in the range 220.0–245.7 pm (corresponding to *Nc* values<sup>[31]</sup> in the

range 0.81–0.97) constrain the atom in place in **1-2a-d** but these interactions might also assist hydrogen hopping between the nitrogen atoms (see below). In co-crystals **1-2b-d**, where  $H^+ \text{crypt-111}$  is more spherical, a quite short H–N hydrogen bond is also present (*Nc* in the range 0.77–0.80).

Consistent with this finding that the proton is bonded to one nitrogen atom, the geometric features at the two N atoms of crypt-111 are different from each other. C–N bond lengths in amines are typically shorter than in respective protonated derivatives and the mean values for such bond lengths at the protonated and non-protonated nitrogen atoms in **1-2a-d** are 145.6 and 149.9 pm, respectively. Consistent with the general trend that protonation enhances the tetrahedral character of an amine nitrogen, the positively charged nitrogen atom in  $H^+ \text{crypt-111}$  shows a smaller mean  $\angle \text{C-N-C}$  angle and a greater distance from the plane through the three bonded carbon atoms than for the neutral nitrogen. (In one of the two independent cations in the crystal of **1-2a** these values are  $112.30^\circ$  vs.  $116.33^\circ$  and 42.5 vs. 28.2 pm, respectively; Table S.4). Finally, in co-crystals **1-2a-d** the iodide anion is invariably closer to one nitrogen atom of crypt-111 than to the other. The positioning of the iodide anion is obviously influenced by the location of the proton and the difference between the two nitrogen–iodide separations is a further indication that the caged proton resides on one nitrogen. Indeed, the mean values of the shortest  $I^- \cdots \text{NH}^+$  and  $I^- \cdots \text{N}$  distances are 464.3 and 608.1 pm, respectively.

### Solid-state $^{15}\text{N}$ NMR characterization of $H^+ \text{crypt-111}$ iodide (**1**) and co-crystal **1-2c**

Solid-state NMR investigations were performed on samples of crypt-111·HI (**1**) and co-crystal **1-2c** to obtain information about the protonation site and the possible occurrence of dynamic processes. Solid-state NMR (SSNMR) can provide clear insights on the proton location by virtue of its inherent multinuclear and multiparametric nature.<sup>[33]</sup> Ultrafast proton transfer rates involving tautomeric equilibria in crystalline powders have been successfully obtained by spin-lattice relaxation measurements with cross-polarization magic angle spinning nuclear magnetic resonance spectroscopy (CPMAS NMR).<sup>[34]</sup> In particular, the  $^{15}\text{N}$  chemical shift is a useful parameter for the location of the hydrogen in protonated nitrogen systems.  $^{15}\text{N}$  NMR is especially suited to study proton transfer in systems involving O–H–N and N–H–N interactions, owing to the fact that the respective nitrogen is directly involved in the H bond, whereas other atoms act as spectators. For example, protonation of aliphatic amines shows upfield shifts  $\Delta\delta$  in the order of 10–25 ppm.<sup>[35]</sup> In Figure 4 the room-temperature  $^{15}\text{N}$  CPMAS NMR spectra of **1** and **1-2c** are assembled. A single line is observed at 30.5 and 32.3 ppm for **1** and **1-2c**, respectively, indicating either an equivalence of the nitrogen atoms arising from a fast proton transfer or from a proton positioned between the two N atoms. To discriminate between the two possibilities a variable-temperature investigation (4–20 K with custom probes) should be performed. Unfortunately such low-temperature experiments are precluded by the very

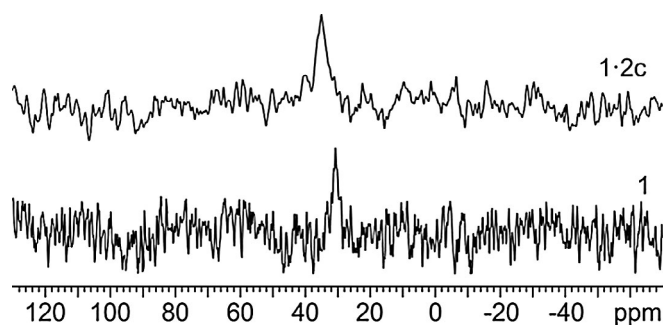


**Figure 4.**  $^{15}\text{N}$  CPMAS spectra (40.56 MHz) of **1** and **1·2c** recorded at a spinning speed of 15 KHz.

long acquisition times required for recording  $^{15}\text{N}$  spectra at natural abundance.

The difference between the proton position and dynamic behavior obtained using X-ray and NMR analyses might not be surprising as it is well known that different conclusions regarding these features can be drawn depending on the time scale of the technique used to probe hydrogen. This is known for the case of enolic tautomerization for acetylacetonate where ultrafast electron diffraction data reveal the presence of an asymmetric structure,<sup>[36]</sup> whereas microwave data clearly show a  $C_{2v}$  symmetry.<sup>[37]</sup> Alternatively, the observed difference might be attributed to the difference in the temperatures of the two experimental procedures.

#### DFT calculations

As suggested above, the single peak for nitrogen atoms in NMR spectra of **1** and the co-crystal **1·2c** could arise from a dynamic process involving the hydrogen hopping from one N atom to the other. However, previous calculations at the HF/6-31G level tend to exclude this interpretation as the corresponding energy barrier was computed as high as  $71\text{ kJ mol}^{-1}$ .<sup>[27]</sup> To shed light on these contrasting indications, we performed DFT calculations at a higher level, namely with the DFT method B97-D3 and the aug-cc-pVDZ basis set. This approach, that includes the D3 version of Grimme's dispersion method with the Becke–Johnson damping Scheme, has been suggested to give reasonably good results for hydrogen-bonded systems treated with a double  $\zeta$  basis set.<sup>[38]</sup> A detailed investigation of  $\text{H}^+\text{Ccrypt-111}$  by DFT reveals that in solution the proton internalization is favored and occurs via a low energy barrier ( $3.2\text{ kJ mol}^{-1}$ ) pathway after external protonation at an oxygen atom. The proton bound through a dative-covalent bond to a nitrogen atom inside the cage is at an energy minimum and the proton hopping between the two N atoms proceeds with an energy barrier of  $11.8\text{ kJ mol}^{-1}$  (see the Supporting Information).

Solid-state DFT calculations, by means of Quantum Espresso, were performed on the crystal structure of **1**. The  $P6_3/m$  hexagonal cell (No. 176) contains two  $\text{H}^+\text{Ccrypt-111}$  cations per unit cell where the proton is covalently bound to one nitrogen but the positions are randomized through orientational disorder of  $\text{H}^+\text{Ccrypt-111}$  cation. This random location results in four dif-

ferent unit cells, namely four couples of  $\text{H}^+\text{Ccrypt-111}$  cations, differing from each other in the relative position of the proton. The N atoms can be protonated (Type 1) or not protonated (Type 0) and the four possible unit cells can be represented as 0101, 1010, 0110, and 1001. For example, in the 0101 cell (Figure 5) the *endo*-protonation occurs at N2 and N4

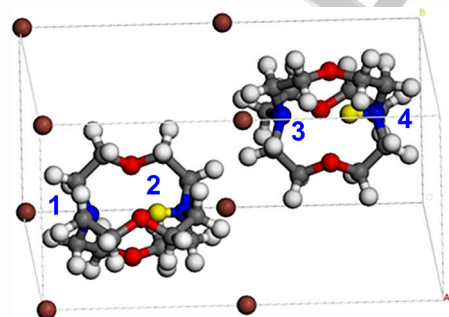


**Figure 5.** The optimized structure (0101) of **1**. Numbering of nitrogen atoms is in blue. Color code for atoms: Gray, carbon; white, hydrogen atoms outside the cage; yellow, hydrogen atoms inside the cage; red, oxygen; blue, nitrogen; brown, iodine.

(if N atoms are numbered from left to right, from 1 to 4). All the four possible structures were optimized, and the geometries were almost identical to the starting randomized cell. The calculations converged into two couples of two equivalent cells, the 0101–1010 couple being  $16\text{ kJ mol}^{-1}$  lower in energy than the 0110–1001 couple. The 0101 cell is used for the rest of the discussion.

The internal transfer of the proton between the two N atoms was computationally investigated in the solid state by means of the Nudged Elastic Band calculations, adopting the “climbing image” optimization Scheme, as implemented in Quantum Espresso. The process occurs via a “breathing” pathway, similar to that outlined for the cation in solution (see the Supporting Information). However, in this case complications arise from the presence of two molecules in the cell. Two types of transition states are possible and they can be better understood by inspecting Figure 5. If the proton transfer involves N1 and N2 (the transfer between N3 and N4 being excluded), the first transition state is associated with the transformation of 0101 into 1001 (0101→1001 process) and corresponds to an activation energy of  $42.6\text{ kJ mol}^{-1}$ . The second transition state is associated with the inverse proton transfer (1001→0101 process) and the corresponding activation energy is  $27.2\text{ kJ mol}^{-1}$ . The difference between the two transition states is mainly influenced by different stabilities of the two couples of conformers. Similar considerations are applied to Nudged Elastic Band calculations of **1·2c**. In this co-crystal, the activation barriers are  $11.3$  and  $4.2\text{ kJ mol}^{-1}$  for the 0101→1001 and 1001→0101 processes, respectively. Although the energy barrier values for **1·2c** are somewhat compatible with the proton dynamic motion suggested by SSNMR, in the case of **1** they are too high.

Previous studies indicated that several parameters need to be considered in the modelling of proton location and dynam-

ics. The strength and symmetry of the hydrogen bond(s) involving a proton are often qualitatively correlated with the average hydrogen bond length<sup>[39]</sup> and are key properties influencing the dynamic behavior of the proton. Other influential features are the quantum nature of the proton, the zero-point motion, the quantum delocalization, and the quantum tunneling.<sup>[11a,40]</sup> It has been found that proton tunneling accounted for the low energy barrier (in comparison with the computed one) unclear, aren't both systems computed? of the *trans-trans* isomerization in hydrogen-bonded porphycene,<sup>[16]</sup> a system with proton dynamism similar to that for **1**. Although the optimized structure of **1** shows a relatively large value of the intramolecular N–N distance, we found that shortening of the N–N distance, accessible through thermal motion, lowers the energy barrier of the proton hopping both in the solid state (NEB calculations) and in solution. This strengthens the intramolecular hydrogen bond (see the Supporting Information), which may favor a possible proton tunneling. If tunneling does occur, it might enable the proton hopping in **1**.

## Conclusion

X-ray data indicate that in both **1** and the three-component co-crystals **1-2a-d** the proton that is encapsulated within the cavity of crypt-111 is covalently bonded to a single nitrogen atom, and is further involved in a network of intramolecular N–H...O and/or N–H...N hydrogen bonds. Crystallographic data also indicate that the geometry at the two N atoms of crypt-111 is the same in **1** but different in **1-2a-d**. On the other hand <sup>15</sup>N solid-state NMR spectra clearly points to the magnetic equivalency of the two N atoms of crypt-111 in both **1** and **1-2c**. Modeling confirms that protonation inside the cavity is favored, that the acidic hydrogen sits preferentially along the internitrogen axis, and the hydrogen is covalently bonded to one nitrogen. The computed energy barriers suggest that hopping of the caged proton between the two N atoms of the cage can occur in the halogen bonded co-crystal **1-2c** but it cannot in the pure H<sup>+</sup>crypt-111 iodide **1**.

A plausible rationalization of the unique structure of H<sup>+</sup>crypt-111 cation in crystalline **1** (where the proton is covalently bound to one N atom, even though crypt-111 has a mirror plane bisecting three O atoms) is that the symmetric conformation of the cryptand arises from a combination of 1) the tendency of the proton to be covalently bound to one nitrogen, 2) the flat conformational landscape of H<sup>+</sup>crypt-111 cation, and 3) the overall packing requirements in the crystal. In other words, in accord with modelling indications that H<sup>+</sup>crypt-111 can undergo conformational change with minor energy variations, minimization of the crystallization energy occurs when the high symmetry of the packing and of the anion lattice elicits a symmetrical conformation for H<sup>+</sup>crypt-111 cation so that orientational disorder in the symmetric anion lattice is favored. The conformation adopted by H<sup>+</sup>crypt-111 cation in **1** is thus a fine example of mutually induced fitting.

As a consequence of the confined space of the cavity of crypt-111, the proton in H<sup>+</sup>crypt-111 cation is proven to have

unique features in the solid state; the flat conformational landscape of the cryptand, the resulting tunable internitrogen distance, and the variable network of hydrogen bonds involving the proton all playing a role in the proton location and dynamic behavior.

Finally it is interesting to observe that in co-crystals **1-2a-d** iodide anions are effectively involved in the formation of short and directional halogen bonds.<sup>[29]</sup> To our knowledge, this is the first indication that the naked iodide anions generated by crypt-111 upon interaction with hydrogen iodide are as nucleophilic as those generated by crypt-222 from alkaline iodides. This finding may open the way for numerous and useful synthetic opportunities.

## Acknowledgements

V. K., T. P., and G. R. gratefully acknowledge financial support from Fondazione Cariplo (Project no. RFJ4RIST01). M.R.C., R.G. and C.N. are indebted with Jeol Company for helpful technical assistance and cooperation.

## Conflict of interest

The authors declare no conflict of interest.

**Keywords:** cryptands · halogen bonding · hydrogen bonding · molecular self-assembly

- [1] a) L. Dong, P. N. Liu, N. Lin, *Acc. Chem. Res.* **2015**, *48*, 2765–2774; b) L. Piot, D. Bonifazi, P. Samori, *Adv. Funct. Mater.* **2007**, *17*, 3689–3693.
- [2] a) C. Li, T. Sato, Y. Yamauchi, *Angew. Chem. Int. Ed.* **2013**, *52*, 8050–8053; *Angew. Chem.* **2013**, *125*, 8208–8211; b) M. Chen, T. Pica, Y.-B. Jiang, P. Li, K. Yano, J. P. Liu, A. K. Datye, H. Fan, *J. Am. Chem. Soc.* **2007**, *129*, 6348–6349.
- [3] a) H. Takezawa, T. Murase, G. Resnati, P. Metrangolo, M. Fujita, *Angew. Chem. Int. Ed.* **2015**, *54*, 8411–8414; *Angew. Chem.* **2015**, *127*, 8531–8534; b) M. G. Sarwar, D. Ajami, G. Theodorakopoulos, I. D. Petsalakis, J. Rebek, Jr., *J. Am. Chem. Soc.* **2013**, *135*, 13672–13675.
- [4] a) A. Galana, P. Ballester, *Chem. Soc. Rev.* **2016**, *45*, 1720–1737; b) P. Mal, B. Breiner, K. Rissanen, J. R. Nitschke, *Science* **2009**, *324*, 1697–1699.
- [5] S. Sambasivan, S.-G. Kim, S. M. Choi, Y. M. Rhee, K. H. Ahn, *Org. Lett.* **2010**, *12*, 4228–4231.
- [6] J. Guo, Y.-W. Xu, K. Li, L.-M. Xiao, S. Chen, K. Wu, X.-D. Chen, Y. Z. Fan, J.-M. Liu, C.-Y. Su, *Angew. Chem. Int. Ed.* **2017**, *56*, 3852–3856; *Angew. Chem.* **2017**, *129*, 3910–3914.
- [7] a) D. Zhang, K. Jamieson, L. Guy, G. Gao, J.-P. Dutasta, A. Martinez, *Chem. Sci.* **2017**, *8*, 789–794; b) S. H. A. M. Leenders, R. G. Doria, B. D. Bruin, J. N. H. Reek, *Chem. Soc. Rev.* **2015**, *44*, 433–448.
- [8] M. Ramanathan, S. M. Kilbey II, Q. Ji, J. P. Hill, K. Ariga, *J. Mater. Chem.* **2012**, *22*, 10389–10405.
- [9] a) Y. Matsuda, T. Mitsuhashi, S. Lee, M. Hoshino, T. Mori, M. Okada, H. Zhang, F. Hayashi, M. Fujita, I. Abe, *Angew. Chem. Int. Ed.* **2016**, *55*, 5785–5788; *Angew. Chem.* **2016**, *128*, 5879–5882; b) Y. Inokuma, S. Yoshioka, J. Ariyoshi, T. Arai, Y. Hitora, K. Takada, S. Matsunaga, K. Rissanen, M. Fujita, *Nature* **2013**, *495*, 461–466.
- [10] V. Duplan, M. Hoshino, W. Li, T. Honda, M. Fujita, *Angew. Chem. Int. Ed.* **2016**, *55*, 4919–4923; *Angew. Chem.* **2016**, *128*, 5003–5007.
- [11] a) W. Liu, Y. Wang, L. Tang, B. G. Oscar, L. Zhu, C. Fang, *Chem. Sci.* **2016**, *7*, 5484–5494; b) C. Drechsel-Grau, D. Marx, *Angew. Chem. Int. Ed.* **2014**, *53*, 10937–10940; *Angew. Chem.* **2014**, *126*, 11117–11120.



- [12] a) J. R. Mohrig, *Acc. Chem. Res.* **2013**, *46*, 1407–1416; b) D. R. Weinberg, C. J. Gagliardi, J. F. Hull, C. F. Murphy, C. A. Kent, B. C. Westlake, A. Paul, D. H. Ess, D. G. McCafferty, T. J. Meyer, *Chem. Rev.* **2012**, *112*, 4016–4093.
- [13] a) D. Jacquemin, J. Zúñiga, A. Requena, J. P. Céron-Carrasco, *Acc. Chem. Res.* **2014**, *47*, 2467–2474; b) D. N. Silverman, R. McKenna, *Acc. Chem. Res.* **2007**, *40*, 669–675.
- [14] a) Y. Ren, A. A. Banishev, K. S. Suslick, J. S. Moore, D. D. Dlott, *J. Am. Chem. Soc.* **2017**, *139*, 3974–3977; b) O. Gerlits, T. Wymore, A. Das, C.-H. Shen, J. M. Parks, J. C. Smith, K. L. Weiss, D. A. Keen, M. P. Blakeley, J. M. Louis, P. Langan, I. T. Weber, A. Kovalevsky, *Angew. Chem. Int. Ed.* **2016**, *55*, 4924–4927; *Angew. Chem.* **2016**, *128*, 5008–5011.
- [15] a) D. Muñoz-Santiburcio, D. Marx, *Nat. Commun.* **2016**, *7*, 12625; b) B. Chatelet, L. Joucla, J.-P. Dutasta, A. Martinez, V. Dufaud, *Chem. Eur. J.* **2014**, *20*, 8571–8574; c) D.; d) P. Adelroth, P. Brzezinski, *Biochim. Biophys. Acta Bioenerg.* **2004**, *1655*, 102–115. ■■■lit b was twice in ref. + lit c is incomplete; changed labelling now (marked in red); please check ■■■
- [16] P. Ciączka, P. Fita, A. Listkowski, C. Radzewicz, J. Waluk, *J. Phys. Chem. Lett.* **2016**, *7*, 283–288. ■■■please check reference and update if needed ■■■
- [17] a) J. Cheney, J.-M. Lehn, *J. Chem. Soc. Chem. Commun.* **1972**, 487–489; b) J. Cheney, J. P. Kintzinger, J.-M. Lehn, *Nouv. J. Chim.* **1978**, *2*, 411–418; ■■■please check reference and update if needed ■■■. c) P. B. Smith, J. L. Dye, J. Cheney, J.-M. Lehn, *J. Am. Chem. Soc.* **1981**, *103*, 6044–6048.
- [18] R. Geue, S. H. Jacobson, R. Pizer, *J. Am. Chem. Soc.* **1986**, *108*, 1150–1155.
- [19] a) G. Alibrandi, V. Amendola, G. Bergamaschi, R. Dollenz, L. Fabbri, M. Lichelli, C. Lo Vecchio, *Chem. Eur. J.* **2013**, *19*, 3729–3734; b) G. Alibrandi, C. Lo Vecchio, A. Villari, I. Villari, *Chem. Eur. J.* **2010**, *16*, 7700–7703; c) G. Alibrandi, C. L. Vecchio, G. Lando, *Angew. Chem. Int. Ed.* **2009**, *48*, 6332–6334; *Angew. Chem.* **2009**, *121*, 6450–6452.
- [20] a) G. Alibrandi, D. G. Lister, C. Lo Vecchio, M. Maeder, *New J. Chem.* **2014**, *38*, 561–567; b) G. Alibrandi, C. G. Arena, G. Lando, *Chem. Eur. J.* **2011**, *17*, 1419–1422.
- [21] Coordinates are available in CSD for only the *exo*-complex of crypr-111 with BF<sub>3</sub>, (refcode ZOXPB; B. Metz, R. Weiss, *New J. Chem.* **1978**, *2*, 615–622). ■■■please check reference and update if needed ■■■
- [22] H.-J. Bruegge, D. Carboo, K. von Deuten, A. Knochel, J. Kopf, W. Dreisig, *J. Am. Chem. Soc.* **1986**, *108*, 107–112.
- [23] a) I. Majerz, I. Olovsson, *Phys. Chem. Chem. Phys.* **2009**, *11*, 1297–1302; b) A. Parkin, K. Wozniak, C. C. Wilson, *Cryst. Growth Des.* **2007**, *7*, 1393–1398.
- [24] J. F. Kögel, X. Xie, E. Baal, D. Gesevičius, B. Oelkers, B. Kovačević, J. Sundermeyer, *Chem. Eur. J.* **2014**, *20*, 7670–7685.
- [25] V. Moliner, I. H. Williams, *J. Am. Chem. Soc.* **2000**, *122*, 10895–10902.
- [26] a) P. L. Anelli, F. Montanari, S. Quici, *J. Org. Chem.* **1985**, *50*, 3453–3457; b) R. Annunziata, F. Montanari, S. Quici, M. T. Vitali, *J. Chem. Soc. Chem. Commun.* **1981**, 777–778.
- [27] R. C. Boehm, R. J. Rencsok, J. F. Harrison, T. A. Kaplan, *J. Phys. Chem.* **1994**, *98*, 6967–6971.
- [28] G. R. Desiraju, P. S. Ho, L. Kloo, A. C. Legon, R. Marquardt, P. Metrangolo, P. Politzer, G. Resnati, K. Rissanen, *Pure Appl. Chem.* **2013**, *85*, 1711–1713. ■■■please check reference and update if needed ■■■.
- [29] a) V. Kumar, T. Pilati, G. Terraneo, F. Meyer, P. Metrangolo, G. Resnati, *Chem. Sci.* **2017**, *8*, 1801–1810; b) G. Cavallo, P. Metrangolo, T. Pilati, G. Resnati, M. Ursini, G. Terraneo, *Acta Crystallogr. Sect. E* **2013**, *69*, m387–388; c) P. Metrangolo, F. Meyer, T. Pilati, G. Resnati, G. Terraneo, *Chem. Commun.* **2008**, 1635–1637; d) D. B. Fox, R. Liantonio, P. Metrangolo, T. Pilati, G. Resnati, *J. Fluorine Chem.* **2004**, *125*, 271–281; e) R. Liantonio, P. Metrangolo, T. Pilati, G. Resnati, *Cryst. Growth Des.* **2003**, *3*, 355–361; f) G. Cavallo, S. Biella, J. Lu, P. Metrangolo, T. Pilati, G. Resnati, G. Terraneo, *J. Fluorine Chem.* **2010**, *131*, 1165–1172; g) R. Liantonio, P. Metrangolo, F. Meyer, T. Pilati, W. Navarrini, G. Resnati, *Chem. Commun.* **2006**, 1819–1821.
- [30] R. D. Walsh, J. M. Smith, T. W. Hanks, W. T. Pennington, *Cryst. Growth Des.* **2012**, *12*, 2759–2768.
- [31] The normalized contact *N<sub>c</sub>* is defined as the ratio  $D_{xy}/(r_X + r_Y)$ , where *D<sub>xy</sub>* is the experimental distance between the halogen bonded iodine atoms X and halide anion Y and *r<sub>X</sub>* and *r<sub>Y</sub>* are the van der Waals radius for iodine and the Pauling ionic radius of the iodide anion Y, respectively. *N<sub>c</sub>* is a useful indicator of the relative interaction strength—more useful than the XB distance itself—because it allows distances between different interacting sites to be compared.
- [32] a) V. Ojogun, B. L. Knutson, S. Vyas, H. J. Lehmle, *J. Fluorine Chem.* **2010**, *131*, 784–790; b) E. de Wolf, P. Ruelle, J. van den Broeke, B.-J. Deelman, G. van Koten, *J. Phys. Chem. B* **2004**, *108*, 1458–1466; c) L. E. Kiss, I. Kövesdi, J. Rábai, *J. Fluorine Chem.* **2001**, *108*, 95–109.
- [33] a) M. R. Chierotti, R. Gobetto, *CrystEngComm* **2013**, *15*, 8599–8612; b) M. U. Schmidt, J. Brüning, J. Glinemann, M. W. Hützel, P. Mörschel, S. N. Ivashevskaya, J. van de Streek, D. Braga, L. Maini, M. R. Chierotti, R. Gobetto, *Angew. Chem. Int. Ed.* **2011**, *50*, 7924–7926; *Angew. Chem.* **2011**, *123*, 8070–8072; c) M. R. Chierotti, L. Ferrero, N. Garino, R. Gobetto, L. Pellegrino, D. Braga, F. Grepioni, L. Maini, *Chem. Eur. J.* **2010**, *16*, 4347–4358.
- [34] a) J. M. Lopez del Amo, U. Langer, V. Torres, G. Buntkowsky, H.-M. Vieth, M. P. Torralba, D. Sanz, R. M. Claramunt, J. Elguero, H.-H. Limbach, *J. Am. Chem. Soc.* **2008**, *130*, 8620–8632; b) C.-G. Hoelger, W. J. Wehrle, H. Benedict, H.-H. Limbach, *J. Phys. Chem.* **1994**, *98*, 843–851.
- [35] a) G. C. Levy, R. L. Lichter, *Nitrogen-15 Nuclear Magnetic Resonance Spectroscopy*, John Wiley & Sons, New York, **1979**; b) M. R. Chierotti, R. Gobetto, *Chem. Commun.* **2008**, 1621–1634.
- [36] W. Caminati, J.-U. Grabow, *J. Am. Chem. Soc.* **2006**, *128*, 854–857.
- [37] U. Langer, C. Hoelger, B. Wehrle, L. Latanowicz, E. Vogel, H.-H. Limbach, *J. Phys. Org. Chem.* **2000**, *13*, 23–34.
- [38] L. A. Burns, A. Vázquez-Mayagoitia, B. G. Sumpter, C. D. Sherrill, *J. Chem. Phys.* **2011**, *134*, 084107–084125.
- [39] a) X.-Z. Li, B. Walker, A. Michaelides, *Proc. Natl. Acad. Sci. USA* **2011**, *108*, 6369–6373; b) M. E. Tuckerman, D. Marx, M. L. Klein, M. Parrinello, *Science* **1997**, *275*, 817–820.
- [40] R. Srinivasan, J. S. Feenstra, S. T. Park, S. Xu, A. H. Zewail, *J. Am. Chem. Soc.* **2004**, *126*, 2266–2267.
- [41] CCDC 1543952 (1), 1543956 (1·2a), 1543954 (1·2b), 1543955 (1·2c), and 1543953 (1·2d) contain the supplementary crystallographic data for this paper. These data are provided free of charge by The Cambridge Crystallographic Data Centre.

Manuscript received: April 16, 2017

Revised manuscript received: June 27, 2017

Accepted manuscript online: June 28, 2017

Version of record online: ■■■■■, 0000

## FULL PAPER

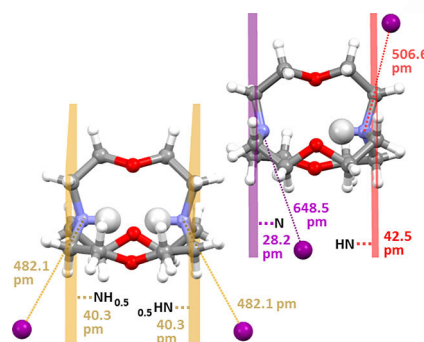
## Crystal Engineering

V. Kumar, T. Pilati, S. Quicik,  
M. R. Chierotti, C. Nervi, R. Gobetto,  
G. Resnati\*

■ ■ - ■ ■



**Proton in a Confined Space: Synthesis  
of H<sup>+</sup>⊂Crypt-111 Iodide and some  
Halogen-Bonded Derivatives**



**H-hop on lockdown:** Experimental observations and modeling data are reported on the solid-state structural features of crypt-111-I (1) and the three-component co-crystals that 1 forms with  $\alpha,\omega$ -diiodoperfluoroalkanes 2 a–d. X-ray analyses indicate that the caged proton is covalently bonded to a single nitrogen atom at room temperature. In contrast, room-temperature, solid-state <sup>15</sup>N NMR spectroscopy suggests magnetic equivalency of the two N atoms of crypt-111 in both 1 alone and co-crystallized with diiodoperfluoroalkanes.

■ ■



H in a cage: Resnati et al. prepare a #cryptand structure and elucidate the nature of proton binding **SPACE**  
RESERVED FOR IMAGE AND LINK

Share your work on social media! *Chemistry - A European Journal* has added Twitter as a means to promote your article. Twitter is an online microblogging service that enables its users to send and read text-based messages of up to 140 characters, known as “tweets”. Please check the pre-written tweet in the galley proofs for accuracy. Should you or your institute have a Twitter account, please let us know the appropriate username (i.e., @accountname), and we will do our best to include this information in the tweet. This tweet will be posted to the journal’s Twitter account @ChemEurJ (follow us!) upon online publication of your article, and we recommended you to repost (“retweet”) it to alert other researchers about your publication.

Please check that the ORCID identifiers listed below are correct. We encourage all authors to provide an ORCID identifier for each coauthor. ORCID is a registry that provides researchers with a unique digital identifier. Some funding agencies recommend or even require the inclusion of ORCID IDs in all published articles, and authors should consult their funding agency guidelines for details. Registration is easy and free; for further information, see <http://orcid.org/>.

Dr. Vijith Kumar <http://orcid.org/0000-0003-0508-3944>  
Dr. Tullio Pilati  
Dr. Silvio Quicik  
Dr. Michele R. Chierotti  
Dr. Carlo Nervi  
Dr. Roberto Gobetto  
Dr. Giuseppe Resnati <http://orcid.org/0000-0002-0797-9296>